Animal Nutrition 8 (2022) 265–276

Contents lists available at ScienceDirect

Animal Nutrition

journal homepage: http://www.keaipublishing.com/en/journals/aninu/

Short Communication

Changes in progenitors and differentiated epithelial cells of neonatal piglets

Lanmei Yin [a, b, c, 1], Jun Li [a, d, 1], Yitong Zhang [a], Qing Yang [a], Cuiyan Yang [a], Zhenfeng Yi [a], Yuebang Yin [b], Qiye Wang [a], Jianzhong Li [a], Nengshui Ding [d], Zhigang Zhang [d], Huansheng Yang [a, b, *], Yulong Yin [a, b, c, *]

[a] Hunan International Joint Laboratory of Animal Intestinal Ecology and Health, Laboratory of Animal Nutrition and Human Health, College of Life Sciences, Hunan Normal University, Changsha, Hunan, 410081, China
[b] Hunan Provincial Key Laboratory of Animal Nutritional Physiology and Metabolic Process, Scientific Observing and Experimental Station of Animal Nutrition and Feed Science in South-Central, Ministry of Agriculture, Hunan Provincial Engineering Research Center for Healthy Livestock and Poultry Production, Key Laboratory of Agro-ecological Processes in Subtropical Region, Institute of Subtropical Agriculture, Chinese Academy of Sciences, Changsha, Hunan, 410125, China
[c] National Center of Technology Innovation for Synthetic Biology, Tianjin Institute of Industrial Biotechnology, Chinese Academy of Sciences, Tianjin, 300308, China
[d] State Key Laboratory of Food Safety Technology for Meat Products, Yinxiang Group, Fujian Aonong Biological Science and Technology Group Co., Ltd., Key Laboratory of Swine Nutrition and Feed Science of Fujian Province, Aonong Group, Zhangzhou, Fujian, 363000, China

ARTICLE INFO

Article history:
Received 19 February 2021
Received in revised form
6 October 2021
Accepted 18 October 2021
Available online 27 November 2021

Keywords:
Fetal type of progenitor
Adult intestinal stem cell
Differentiated epithelial cell
Neonatal piglet

ABSTRACT

This study aimed to assess the changes of small intestinal morphology, progenitors, differentiated epithelial cells, and potential mechanisms in neonatal piglets. Hematoxylin and eosin staining of samples from 36 piglets suggested that dramatic changes were observed in the jejunum crypts depth and crypt fission index of neonatal piglets ($P < 0.001$). The number of intestinal stem cells (ISC) tended to increase ($P < 0.10$), and a decreased number of enteroendocrine cells appeared in the jejunal crypt on d 7 ($P < 0.05$). Furthermore, the mRNA expression of jejunal *chromogranin A* (*ChgA*) was down-regulated in d 7 piglets ($P < 0.05$). There was an up-regulation of the adult ISC marker gene of SPARC related modular calcium binding 2 (*Smoc2*), and Wnt/β-catenin target genes on d 7 ($P < 0.05$). These results were further verified in vitro enteroid culture experiments. A mass of hollow spheroids was cultured from the fetal intestine of 0-d-old piglets ($P < 0.001$), whereas substantial organoids with budding and branching structures were cultured from the intestine of 7-d-old piglets ($P < 0.001$). The difference was reflected by the organoid budding efficiency, crypt domains per organoid, and the surface area of the organoid. Furthermore, spheroids on d 0 had more Ki67-positive cells and enteroendocrine cells ($P < 0.05$) and showed a decreasing trend in the ISC and goblet cells ($P < 0.10$). Moreover, the mRNA expression of spheroids differed markedly from that of organoids, with low expression of intestinal differentiation gene (Lysozyme; $P < 0.05$), epithelial-specific markers (*Villin*, *E-cadherin*; $P < 0.05$), and adult ISC markers (leucine-rich repeat-containing G protein-coupled receptor 5 [*Lgr5*], *Smoc2*; $P < 0.001$), and up-regulation of fetal marker (connexin 43 [*Cnx43*]; $P < 0.05$). The mRNA expression of relevant genes was up-regulated, and involved in Wnt/β-catenin, epidermal growth factor (EGF), Notch, and bone morphogenetic protein (BMP) signaling on d 7 organoids ($P < 0.05$). Spheroids displayed low differentiated phenotype and high proliferation, while organoids exhibited strong differentiation potential. These results indicated that the conversion from the fetal progenitors (spheroids) to adult ISC (normal

* Corresponding authors.
E-mail addresses: yhs@hunnu.edu.cn (H. Yang), yinyulong@isa.ac.cn (Y. Yin).
[1] These authors contributed equally to this work.
Peer review under responsibility of Chinese Association of Animal Science and Veterinary Medicine.

Production and Hosting by Elsevier on behalf of KeAi

https://doi.org/10.1016/j.aninu.2021.10.008

organoids) might largely be responsible for the fast development of intestinal epithelial cells in neonatal piglets.

1. Introduction

A small number of temporally distinct stem/progenitor cells located at the base of the intestinal crypts support the development and constant renewal of the intestinal epithelium during fetal development and postnatal life (Buczacki et al., 2013; Pont and Yan, 2018). In mice, fetal progenitors are believed to originate in the area of newly formed villi around embryonic d 15 to 16 (E15 to E16) to ensure the rapid expansion of the epithelium (Mustata et al., 2013). Leucine-rich repeat-containing G-protein coupled receptor 5 (Lgr5) intestinal stem cells (ISC) at the base of the crypts support the ongoing renewal of adult tissues, where the adult ISC divide to generate stem cells and transit-amplifying (TA) daughter cells that further differentiate into one of the absorptive (enterocytes) or secretory cell lineages (Paneth cells, goblet cells, and enteroendocrine cells) (Jones and Dempsey, 2016). A recent study found that the intestinal epithelium in mice is generated from different kinds of progenitors in 2 successive stages, namely, connexin 43 positive ($Cnx43^{+}$) cells in the transient fetal stage and the $Lgr5^{+}$ precursors of the crypt base columnar (CBC) cells in the postnatal stage (Mustata et al., 2013). Taken together, fetal progenitors and $Lgr5^{+}$ ISC play different roles in mouse intestinal development and maintenance of intestinal function. However, the applicability of this finding to pigs remains to be explored.

The continual and rapid intestinal renewal and maturation is a critical period of intestinal development of piglets, which will affect the digestion and absorption of nutrients, intestinal health, and growth performance (Yang et al., 2013; Yan et al., 2018). Accordingly, the elucidation of the mechanism of intestinal development is the key to regulating intestinal epithelium development. Importantly, the functional and developmental differences between fetal progenitors and $Lgr5^{+}$ ISC suggested the potential of nutrients to regulate the conversion of ISC. Consequently, the investigation into changes of ISC populations will provide a vital theoretical basis for nutritional regulation of intestinal development in piglets.

Since organoids have long been used as in vitro models in numerous nutritional studies on intestinal epithelial renewal and development (Pierson et al., 2019; Yin et al., 2019b), the intestinal organoid is a good model for isolating and characterizing the epithelial progenitors of the small intestine in the fetus and postnatal life of pigs. However, it remains unclear how the ISC niche regulates cell fate and differentiation. Increasing evidence suggests that several signaling pathways, including Wnt, epidermal growth factor (EGF), and Notch pathways, which are all active in ISC, and the bone morphogenetic protein (BMP) pathway, inhibited in ISC, are involved in maintaining and regulating the balance between self-renewal and lineage differentiation of ISC (Yeung et al., 2011; Beumer and Clevers, 2021). The intestinal epithelium of neonatal piglets develops rapidly (Pu et al., 2018), which may be associated with changes in progenitors. To verify this hypothesis, changes in small intestinal morphology, progenitors, differentiated epithelial cells, and underlying mechanisms in neonatal piglets of different ages were analyzed, which is expected to promote the understanding of the mechanism of piglet intestinal development.

2. Materials and methods

2.1. Animals and animal ethics

The experimental protocol was reviewed and approved (Approval number 2016-093) by the Animal Care and Use Committee of Hunan Normal University, Changsha City, Hunan, China (Yin et al., 2020). A total of 36 newborn boar piglets (Duroc × [Landrace × Yorkshire]) of similar BW were selected from 9 sows (4 piglets per sow), and the piglets from the same sow were randomly assigned to 2 groups (2 piglets per group). All piglets were fed with sow milk. The intestinal morphology of all piglets was measured, and the ISC activity of 8 piglets was evaluated.

2.2. Sampling

The piglets were euthanized in 2 equal groups with 4% sodium pentobarbital solution on postnatal d 0 and 7 (Ren et al., 2014). The small intestine was removed, and the duodenum, jejunum, and ileum were separated and immediately irrigated with physiological saline to remove the intestinal contents. An approximately 2-cm intestinal segment was fixed in 4% neutral-buffered formalin and stored at 4 °C before morphology measurements.

2.3. Morphological analysis

The paraffin sections were made through dehydration, transparency, wax dipping, and embedding according to previous studies (Wang et al., 2020b). The villus height (VH), villus width, and crypt depth (CD) were measured, and the ratio of villus height to crypt depth (VH:CD) was calculated (Li et al., 2019a). Each measurement was taken by averaging the values of at least 30 well-oriented, intact villus–crypt structures. The number of crypts in fission was determined by observing at least 100 crypts per piglet for a bifurcation with a fissure creating 2 flask-shaped bases with a shared single crypt–villus junction. The number of crypts per circumference was counted on intact transverse sections. The crypt fission index was calculated as the ratio of the number of crypts in fission to the total crypt number (Park et al., 1997; Dehmer et al., 2011).

2.4. Porcine crypt isolation, ex vivo cultivation and measurement

Enteroids, also known as mini-guts, are organoid 3D cells cultured from ISC or intestinal crypts. However, porcine organoids cannot be cultured with the same method as human and murine enteroids due to the differences among the 3 species (Khalil et al., 2016; Powell and Behnke, 2017). The porcine intestinal epithelium has greater CD and extremely abundant villi, and it is challenging to obtain purified and structurally intact crypts.

A 3-cm segment of the proximal jejunum best for organoid growth was removed and immediately irrigated with ice-cold PBS (HyClone) to remove the intestinal contents. Fat and mesentery attached to the jejunum were removed with forceps and scissors. Then, the jejunum was cut longitudinally and washed with ice-cold PBS. The mucosal surface was scraped with a coverslip to remove

the villi (Khalil et al., 2016). Then, the jejunum was cut into small sections of 2 to 4 mm and transferred into a 50 mL conical tube with 15 mL cold PBS. The jejunum sections were pipetted up and down 3 times with a pre-rinsed serological pipette. After repeating the pipetting process 15 to 20 times, the sections were re-suspended in 30 mL PBS. Then, ethylene diamine tetraacetic acid (EDTA; Sigma–Aldrich) was added to adjust the final concentration to approximately 2 mmol/L. The tube was then placed on a rotator to incubate at 4 °C, 50 × *g* for 60 min. After incubating, the tube was set on ice for 5 min to let the sections settle before pipetting off the supernatant. The sections were then re-suspended by pipetting up and down 20 times with a 5-mL tip. After the settling of the sections, the first fraction of the supernatant was discarded to remove the remaining EDTA. Then, 15 mL PBS was added to the tube, and the content of the tube was pipetted up and down 30 times to release more crypts. After the sections had settled again, the supernatant was aspirated and filtered through a 70-μm cell strainer (BD, 352340) into a new tube. The strainer was discarded, and the tube was labeled as fraction 2. The process was repeated 2 more times to obtain fractions 3 and 4. Then, 10% fetal bovine serum (FBS; Gibco) was added to the fractions that were then centrifuged at 300 × *g* for 5 min. The supernatant was discarded and the crypts were re-suspended in a 2 mL complete medium consisting of advanced DMEM/F12 (Gibco), 1% GlutaMAX Supplement (Gibco), 10 mmol/L HEPES (Gibco), and 100 U/mL penicillin-100 μg/mL streptomycin (Gibco). After centrifugation at 150 × *g* for 5 min, the crypts were pelleted and the medium in the supernatant was discarded. Approximately 400 crypts were suspended in 40 μL of cold Matrigel (Corning). Afterward, a drop of the crypts-containing Matrigel was carefully placed in the center of each well of a pre-warmed 24-well plate and subsequently incubated at 37 °C with 5% CO_2 for 15 min. After the Matrigel solidified, a 500-μL culture medium was added to each well. The culture medium was supplemented with Wnt3a, Noggin, R-spondin1 (WNR) conditioned medium, FBS, N2 supplement (Gibco), B27 supplement (Gibco), n-Acetyl Cysteine (Invitrogen), nicotinamide (Sigma–Aldrich), EGF (Sigma–Aldrich), A83-01 (TGF-beta inhibitor, Tocris), SB202190 (p38 inhibitor, R&D Systems) and Y27632 (Rho-kinase inhibitor, R&D Systems). Adult porcine intestinal crypts are more Wnt-dependent because of the powerful effects of the glycogen synthase kinase 3 inhibitor (GSK3i, CHIR99021) on the forming and survival of enteroids in primary culture (Khalil et al., 2016). The culture media were supplemented with 2.5 μmol/L CHIR99021 (Sigma). Y27632 was only supplied for the first 2 d, and the growth media were refreshed every 2 to 3 d. Photos were taken and measured on d 5 of culture. The organoid activity was determined according to the organoid budding efficiency and crypt domains per organoid (Li et al., 2019b; Zhou et al., 2019). Organoid budding efficiency was calculated as the ratio of budding organoids to total organoids. Organoids touching the edge of the images were not counted, and the statistical analysis of budding efficiency and crypt domains per organoid was based on individual wells (Lindemans et al., 2015).

2.5. RNA extraction and real-time quantitative PCR

The spheroids and organoids grown in the 24-well plate were harvested into 1.5-mL centrifuge tubes with TRIzol after photo-taking on d 5. Total RNA extraction, cDNA synthesis, and real-time quantitative PCR (RT-qPCR) were conducted according to Wang et al. (2020a). Primers for the selected genes in Table 1 were designed on Primer Premier 5.0 (Premier Biosoft International, Palo Alto, CA, USA). Each of the PCR reactions was performed on a QuantStudio 5 RT-PCR System (Thermo Fisher Scientific Inc., Rockford, IL, USA) with 5 μL of SYBR Green mix, 0.3 μL of forward and 0.3 μL of reverse primers respectively, 3.4 μL of sterile double-distilled H_2O, and 1 μL of cDNA. The PCR cycling conditions were: pre-denaturation at 95 °C for 10 s; amplification for 40 cycles at 95 °C for 5 s and at 60 °C for 20 s. The housekeeping gene (*β-actin*) was employed to normalize the expression of the target gene, with the gene expression values being calculated with the $2^{-\triangle\triangle Ct}$ method (Xiong et al., 2015). All samples were prepared in triplicate on each 384-well plate. The values of each duplicate were averaged for subsequent statistical analyses.

Table 1
Primer sequence used for the quantification of mRNA expression by real-time quantitative PCR.

Genes[1]	Primers	Sequences (5′–3′)	Products length, bp
Villin	Forward	ACGTGTCTGACTCCGAGGGAAAGGT	201
	Reverse	ACTGCTTCGCTTTGATAAAGTTCAG	
E-cadherin	Forward	TTCAACCCAACCTCGTACCA	181
	Reverse	CGCCTTCATTGGTTACTGGG	
TJP1	Forward	TTGATAGTGGCGTTGACA	126
	Reverse	CCTCATCTTCATCATCTTCTAC	
Alpi	Forward	GCTCTCCCTTGGCTTCATCC	140
	Reverse	CATCCCCCAGAAAGAAATGAGGTT	
Muc2	Forward	AGACGGGCGGAGACTTTGAATC	102
	Reverse	CTTGGATGGGAACGCTGGGATA	
Lyz	Forward	AATAGCCGCTACTGGTGTAATGATG	148
	Reverse	ATGCTTTAACGCCTAGTGGATCTCT	
ChgA	Forward	CCAGCACCCACCCCTTAGCC	192
	Reverse	CTTCTTCCTCCGGGACCGCC	
Tacstd2	Forward	CATTACGAGCACCCCACCAT	239
	Reverse	GTGAGGCGCTTCATGGAGAA	
Gja1	Forward	TGTTTCCTCTCTCGTCCCAC	143
	Reverse	TCACTCTTTCCCTTCACACGA	
Spp1	Forward	GCCTCTGCCCTTCCAGTTAAA	210
	Reverse	CTCAGGGCTTTCGTTGGACT	
Lgr5	Forward	GCCTTTGTAGGCAACCCTTC	121
	Reverse	AGGCACCATTCAAAGTCAGTG	
Smoc2	Forward	ACGAACAGCCGAAATGTGAC	129
	Reverse	CGTCCAACACACTCGTCAGA	

(*continued on next page*)

Table 1 (*continued*)

Genes[1]	Primers	Sequences (5′–3′)	Products length, bp
Cdx1	Forward	CCGGACCAAGGACAAGTACC	134
	Reverse	GTTCGGTGAGCCCCAGATT	
Notch1	Forward	ACAGCAACCCCTGTATCCAC	202
	Reverse	CAGTTGGGGCCGCTGAAG	
Notch2	Forward	AAACCTGGGAACAGAAGCACT	151
	Reverse	CTCGCAAGGGTCTCGATGT	
Atoh1	Forward	AAAACGAGGAACGCTGAGGT	132
	Reverse	AGTTGAGTTTGTCCCCGAGC	
Hes1	Forward	TCAACGCCATGACCTACCCT	209
	Reverse	GAAGCCGCCGAATACCTTTG	
Dll1	Forward	TGACACTCAGGGGTGGAGAA	158
	Reverse	TCACTGGGACAAGAGCCAAC	
Dll4	Forward	ATCCCCCACAATGGCTGTC	278
	Reverse	TAGCCATCCTCTTGGTCCTTGC	
Jag1	Forward	CAAGTGCATGTGTCCTGGAG	133
	Reverse	TTTGCAGACACACGTGAAGG	
Jag2	Forward	GCACAATACCAACGACTGCA	137
	Reverse	ACTGGCACTCGTCAATGTTG	
Sgk1	Forward	CCGACTTTGGACTCTGCAAG	186
	Reverse	TTCGGCTGTAAAATGGAGGC	
Bmp4	Forward	GCCAGCATGTCAGGATTAGC	169
	Reverse	TTCTTCTTCCGAGCCCTCTG	
Nedd8	Forward	AGACAAGGTGGAGCGAATCA	112
	Reverse	AGCTGCTGTCTTCTCATCGT	
Ephb4	Forward	CTGAGTGAGGCCTCCATCAT	168
	Reverse	GAGCTGGATGACGGTGAACT	
c-Myc	Forward	TCCACGCACCAGCACAATTA	200
	Reverse	TCGTTTCTCCTCTGGCGTTC	
Ccnd1	Forward	CTGACGGCCGAGAAGTTGT	146
	Reverse	TTGGAGAGGAAGTGCTCGAT	
Axin2	Forward	GAGGGAGAAATGCGTGGATA	153
	Reverse	GGTTTCAGCTGCTTGGAGAC	
EGFR	Forward	GGAGATCAGCGACGGAGAC	171
	Reverse	GAGCACAGCGGGTTACAGA	
Id2	Forward	CCCAGCATCCCTCAGAACAAGAAG	121
	Reverse	GGTGGTGCAGGCTGACAATAGTG	
Id1	Forward	ACGACATGAACGGCTGCTATTCTC	124
	Reverse	TCCAACTCCAGGTCCCAGATGTAG	
Smad4	Forward	TGCTGCTGGAATCGGTGTTGATG	101
	Reverse	CCTTGATGCTCTGCCTTGGGTAATC	
Bmp2	Forward	GATCCCAAAGGCGTGCTGTG	122
	Reverse	GACACCCACAACCCTCCACA	
Bmpr1a	Forward	TGTCAAACGTTTGCGGCCAA	98
	Reverse	GATTGTGGGCCCAGCATTCC	
β-actin	Forward	AGTTGAAGGTGGTCTCGTGG	216
	Reverse	TGCGGGACATCAAGGAGAAG	

[1] *TJP1* = tight junction protein 1; *Alpi* = alkaline phosphatase, intestinal; *Muc2* = mucin 2; *Lyz* = lysozyme; *ChgA* = chromogranin A; *Tacstd2* = tumor associated calcium signal transducer 2; *Gja1* = gap junction protein, alpha 1; *Spp1* = secreted phosphoprotein 1; *Lgr5* = leucine-rich repeat-containing G protein-coupled receptor 5; *Smoc2* = SPARC related modular calcium binding 2; *Cdx1* = caudal type homeobox 1; *Notch1* = Notch receptor 1; *Notch2* = Notch receptor 2; *Atoh1* = atonal bHLH transcription factor 1; *Hes1* = hes family bHLH transcription factor 1; *Dll4* = delta like canonical Notch ligand 4; *Dll1* = delta like canonical Notch ligand 1; *Jag1* = jagged canonical Notch ligand 1; *Jag2* = jagged canonical Notch ligand 2; *Sgk1* = serum/glucocorticoid regulated kinase 1; *Bmp4* = bone morphogenetic protein 4; *Nedd8* = neural precursor cell expressed developmentally down-regulated 8; *Ephb4* = EPH receptor B4; *Axin2* = axis inhibition protein 2; *EGFR* = epidermal growth factor receptor; *Ccnd1* = cyclin D1; *Id1* = inhibitor of DNA binding 1; *Id2* = inhibitor of DNA binding 2; *Smad4* = SMAD family member 4; Bmp2 = bone morphogenetic protein 2; *Bmpr1a* = bone morphogenetic protein receptor type 1a.

2.6. Immunohistochemistry

2.6.1. Organoids embedding

The culture medium was removed from the wells and washed with 500 μL PBS without disrupting the Matrigel dome. Then, a 500-μL ice-cold cell recovery solution (Corning) was added to each well that was on a horizontal shaker at 4 °C, 15 × *g* for 30 to 60 min until the 3D drops were dissolved without damaging organoid morphology. Organoids were transferred in a 15 mL conical vial tube, followed by spinning down at 4 °C, 150 × *g* for 5 min. The supernatant was discarded, and 500 μL 4% neutral-formalin was added to the pellet to fix organoids for 30 to 60 min at 4 °C. According to the previous studies, the organoid paraffin sections were made through dehydration, transparency, wax dipping, and embedding (Van Lidth de Jeude et al., 2015; Yin et al., 2015). Sections were cut and incubated at 37 °C overnight.

2.6.2. Sex-determining region Y-box transcription factor 9^{+}(SOX9), Ki67, and chromogranin A (ChgA) immunohistochemistry analysis

The paraffin sections (4 μm) were deparaffinized, rehydrated, and treated with 3% hydrogen peroxide (H_2O_2) in methanol (Wang et al., 2020a). Antigen retrieval was performed by boiling slides twice in 0.01 mol/L sodium citrate (pH 6.0), with each boiling lasting 2 min. Thereafter, nonspecific binding was blocked at 37 °C for 10 min with 5% bovine serum albumin (BSA) diluted at 1:10. Slides were then incubated with the anti-SOX9 antibody (Millipore, Ab5535; 1:1,000), anti-Ki67 (Abcam, ab15580; 1:1,000), anti-CgA antibody (Immunostar, 20086; 1:800) at 37 °C for 1.5 h. After incubation, sections were treated with a goat anti-rabbit IgG secondary antibody (ZSGB-BIO, Beijing, China) at 37 °C for 45 min and labeled with the diaminobenzidine (DAB) Kit (ZSGB-BIO). Sections were counterstained with hematoxylin and dehydrated for measurement. Images were acquired with the Leica Application Suite version 4.0 Software (Leica

DM3000; Wetzlar, Germany). For tissues analysis, the average number of CgA-positive cells in crypt and villus per piglet was determined from at least 30 well-oriented villus-crypt structures, and the SOX9, and Ki67-positive cells in the crypt were calculated from at least 30 intact crypts. Quantification of organoid immunohistochemistry analysis was determined as previously described (Navis et al., 2019; Ito et al., 2020). For enteroids analysis, ISC, proliferation cells, goblet cells, and enteroendocrine cells were quantified as the ratio of the number of positive cells to total cell nuclei stained with hematoxylin per organoid.

2.6.3. Organoid measurement

Organoids were quantified on d 5 of culture. Samples for mRNA and immunohistochemistry analysis were collected from 5 d after isolation. The organoid activity was determined based on the organoid budding efficiency and crypt domains per organoid (Li et al., 2019b; Zhou et al., 2019). After 5 d of culture, total organoid numbers per well were counted by light microscopy to evaluate growth efficiency. The number of all organoids was counted manually. For growth condition evaluation, the surface area of organoid horizontal cross-sections was measured according to the previous study (Lindemans et al., 2015). If all organoids in a well could not be measured, several random non-overlapping pictures were taken from each well using an inverted microscope (DMI 8; Leica) and then counted using Image-Pro Plus 6.0 (Media Cybernetics, San Diego, CA, USA) software. The surface area of organoids was measured using "Magic Wand" (automated size measurement) or "Trace" (manual size measurement). The sizes of the largest and smallest organoids in the reference well were measured manually, and their areas were used as the reference values for setting the minimal and maximal particle sizes. Organoids touching the edge of the images were excluded from the counting.

2.7. Alcian blue-periodic acid-Schiff (AB-PAS) staining

Goblet cells were visualized by staining with AB-PAS staining (Nanjing Jiancheng Bioengineering Institute, Nanjing, China) according to the protocol with the methods described by Deng et al. (2020). The number of goblet cells in the jejunum was counted in at least 30 villi and crypts.

2.8. Statistical analysis

Data were analyzed on IBM SPSS Statistics 22 (SPSS Inc., Chicago, IL, USA). The normality of data distribution was checked with histograms and the Shapiro–Wilk test, with each value departing more than 3 standard deviations from the standardized mean being examined. If the data were not normally distributed, values would be transformed before statistical analysis. Non-parametric testing was performed if normal distribution could not be assumed. Values in the figure were expressed as mean and SEM, and graphs were generated with GraphPad Prism 6.0 (GraphPad Inc., San Diego, CA, USA). Differences were assessed by the Student's *t*-test and denoted as follows: $*P < 0.05$, $**P < 0.01$, $***P < 0.001$.

3. Results

3.1. The small intestinal morphology of neonatal piglets

As shown in Table 2, dramatic changes in gut morphology were observed after birth. Villus height in the jejunum was greatly decreased on d 7 after birth ($P < 0.001$), and CD was significantly increased in the duodenum, jejunum, and ileum in the early postnatal periods ($P < 0.001$), which resulted in a lower VH:CD of the small intestine in neonatal piglets ($P < 0.001$). Moreover, villus width increased enormously in the duodenum ($P < 0.001$), jejunum ($P < 0.05$), and ileum ($P < 0.01$). Total crypt numbers in the duodenum and jejunum did not significantly change after birth ($P > 0.05$), but significantly increased in the ileum ($P < 0.001$). The crypt fission index was greatly reduced in the duodenum and jejunum ($P < 0.001$). Representative images of duodenum, jejunum, and ileum sections are shown in Fig. 1.

Table 2
The morphology of small intestine of neonatal piglets.[1]

Item	Day after birth		*P*-value
	0 d	7 d	
Duodenum			
Villus height, μm	510.20 ± 31.31	476.93 ± 24.98	0.417
Crypt depth, μm	105.90 ± 6.32	182.18 ± 8.68	<0.001
Villus width, μm	67.75 ± 2.58	109.55 ± 3.91	<0.001
VH:CD[3], μm:μm	4.99 ± 0.35	2.80 ± 0.22	<0.001
Total crypt number[2]	174.69 ± 9.81	194.75 ± 3.36	0.167
Crypt fission index, %	23.42 ± 2.16	9.21 ± 0.90	<0.001
Jejunum			
Villus height, μm	690.66 ± 32.11	453.09 ± 35.03	<0.001
Crypt depth, μm	79.07 ± 2.03	151.83 ± 7.62	<0.001
Villus width, μm	80.92 ± 2.43	91.45 ± 3.65	0.048
VH:CD, μm:μm	8.74 ± 0.34	3.11 ± 0.32	<0.001
Total crypt number	166.50 ± 6.82	170.31 ± 4.86	0.646
Crypt fission index, %	8.20 ± 0.55	3.99 ± 0.50	<0.001
Ileum			
Villus height, μm	507.18 ± 38.12	529.50 ± 52.30	0.732
Crypt depth, μm	90.90 ± 6.05	215.46 ± 19.77	<0.001
Villus width, μm	81.89 ± 5.52	107.93 ± 4.95	0.002
VH:CD, μm:μm	5.88 ± 0.53	2.95 ± 0.48	<0.001
Total crypt number	148.36 ± 10.86	194.65 ± 3.35	<0.001
Crypt fission index, %	1.80 ± 0.19	1.39 ± 0.19	0.121

[1] The values are expressed as mean ± SEM ($n = 18$). Differences were assessed by the Student's *t*-test. Values of $P < 0.05$ are referred to as statistically significant.
[2] The number of crypts per circumference was counted on intact transverse sections according to Dehmer et al. (2011).
[3] VH:CD = the ratio of villus height to crypt depth.

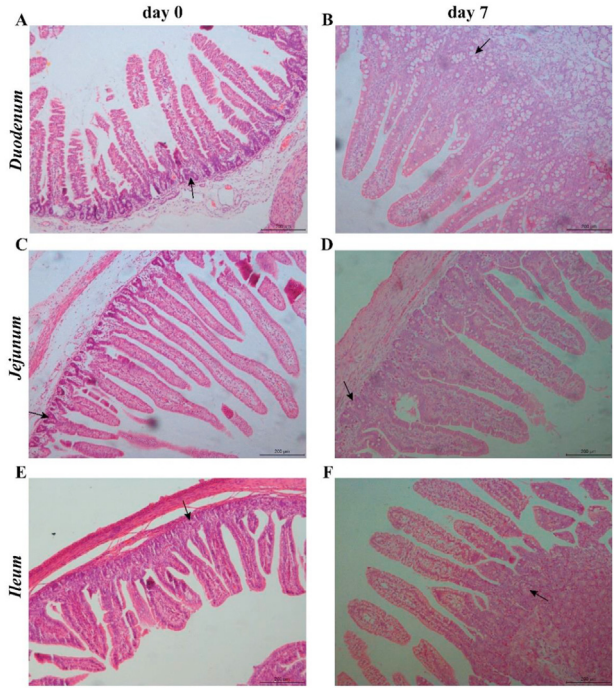

Fig. 1. The small intestinal morphology in d 0 and 7 piglets. Representative images of duodenal, jejunal, and ileal morphology in piglets on d 0 (A, C, and E) and d 7 (B, D, and F) of age (100× magnification; scale bar, 200 μm). Arrows in the figure denote crypt fission.

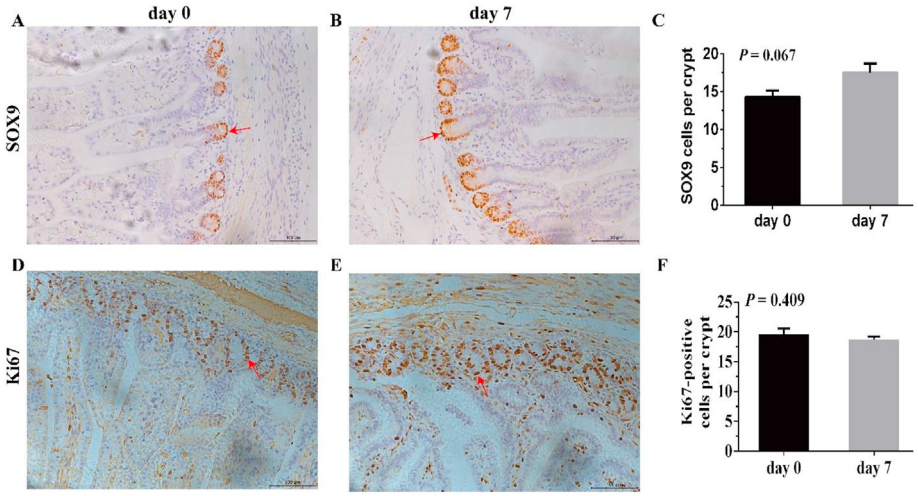

Fig. 2. Intestinal stem cell (ISC) and cell proliferation in the jejunum of d 0 and 7 piglets. Representative immunohistochemical images of piglet jejunum show ISC (A and B) and proliferating cells (D and E) (200× magnification; scale bar, 100 μm). Intestinal stem cells and proliferating cells are dark brown in the crypt using the anti-SOX9, anti-Ki67 antibody respectively and are marked by red arrows. Quantitative analysis of ISC and proliferating cells were displayed (C and F). The values in the figure are expressed as the mean and SEM ($n = 18$); differences were assessed by the Student's *t*-test. Values at $P < 0.10$ show a tendency toward differing.

3.2. Intestinal stem cells, cell proliferation and differentiation in the jejunum of neonatal piglets

SOX9, Ki67-positive cells mark the ISC, enterocyte proliferation respectively, and are located in the crypts. As presented in Fig. 2, in vivo, the number of ISC per crypt showed an increasing trend on d 7 ($P < 0.10$). Moreover, as displayed in Fig. 3, enteroendocrine cells per jejunal crypt of piglets on d 0 increased compared to that on d 7 ($P < 0.05$). And no significant differences were observed in Ki67-positive cells, goblet cells in villus and crypt, as well as enteroendocrine cells in villus ($P > 0.05$). Fig. 2 provided representative images of ISC and cell proliferation, and Fig. 3 Provided representative images of goblet cells and enteroendocrine cells immunohistochemistry from the jejunum.

3.3. Growth, ISC, cell proliferation, and differentiation of jejunal enteroids

As captured in Fig. 4, organoid budding efficiency and crypt domains per organoid on d 7 were significantly increased ($P < 0.001$) compared with d 0, and no significant difference was observed in crypt depth ($P > 0.05$). Moreover, the surface area of organoids on d 7 was significantly greater than d 0 ($P < 0.05$).

As presented in Fig. 5, ISC in organoids on d 7 showed an increasing trend ($P < 0.10$) compared with spheroids on d 0. Moreover, spheroids on d 0 had more Ki67-positive cells than organoids on d 7 ($P < 0.05$).

As shown in Fig. 6, goblet cells in d 7 organoids tended to increase ($P < 0.10$) compared with spheroids on d 0. However, enteroendocrine cells in spheroids on d 0 significantly increased ($P < 0.05$).

3.4. The mRNA expression of related markers in the jejunal tissue of neonatal piglets

As presented in Table 3, the mRNA expression of *ChgA* in the jejunal tissue of piglets on d 7 was down-regulated ($P < 0.05$), as well as tended to down-regulate ($P < 0.10$) the mRNA expression of *Villin* compared to that of piglets on d 0. Moreover, there was an up-regulation of the adult ISC marker gene of SPARC related modular calcium binding 2 (*Smoc2*, $P < 0.05$) on d 7.

3.5. The mRNA expression of related markers in jejunal enteroids

As shown in Table 4, the mRNA expression of *Villin* and *E-cadherin* in the jejunal organoid cultured from piglets on d 7 were up-regulated ($P < 0.05$) compared to that of piglets on d 0. Moreover, there was an up-regulation of the adult ISC marker genes of *Lgr5*, and *Smoc2* ($P < 0.001$) but a down-regulation of fetal ISC marker gene—gap junction protein, alpha 1 (*Gja1*, referred to as *Cnx43*; $P < 0.05$) on d 7. Spheroids appeared on d 0, showed lower mRNA expression of lysozyme (*Lyz*; $P < 0.05$), and were likely to down-regulate the mucin2 (*Muc2*; $P < 0.10$) mRNA expression but significantly up-regulate the *ChgA* expression ($P < 0.05$).

3.6. The mRNA expression of related genes involved in differentiation and self-renewal pathways of jejunal tissue in vivo

As illustrated in Table 5, there was a down-regulation of Wnt/β-catenin target genes on d 7, such as bone morphogenetic protein 4 (*BMP4*), neural precursor cell expressed developmentally down-regulated 8 (*Nedd8*), axis inhibition protein 2 (*Axin2*) ($P < 0.05$) compared to d 0.

3.7. The mRNA expression of related genes involved in differentiation and self-renewal pathways of jejunal enteroids in vitro

As shown in Table 6, the mRNA expression of Wnt/β-catenin target genes, such as jagged canonical Notch ligand 1 (*Jag-1*), jagged canonical Notch ligand 2 (*Jag-2*), *Nedd8*, EPH receptor B4 (*Ephb4*), *c-Myc*, cyclin D1 (*Ccnd1*), and *Axin2*, were up-regulated in the piglets' jejunal tissue on d 7 ($P < 0.05$) compared to that of piglets on d 0. Moreover, there was an up-regulation ($P < 0.05$) of epidermal growth factor receptor (*EGFR*) involved in EGF signaling, Notch receptor 1 (*Notch1*), hes family bHLH transcription factor 1 (*Hes1*) involved in Notch signaling, as well as bone morphogenetic protein receptor type 1a (*Bmpr1a*), SMAD family member 4 (*Smad4*) involved in BMP signaling on d 7.

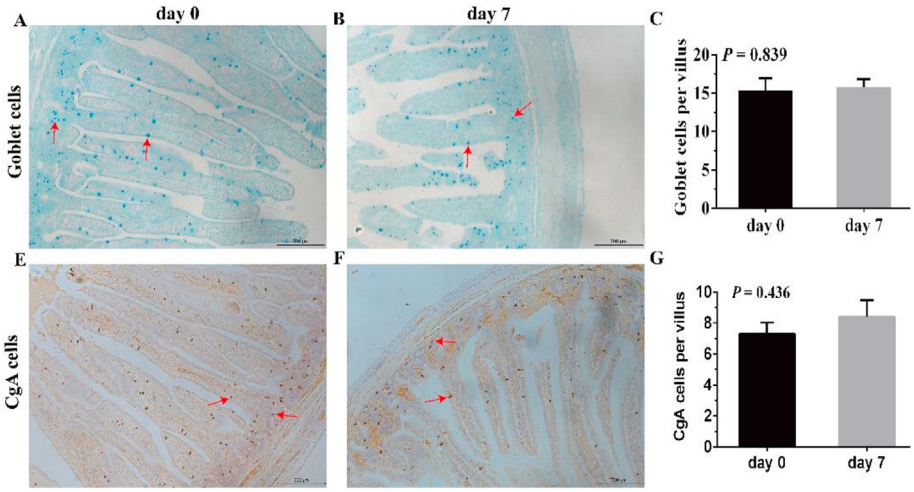

Fig. 3. Goblet cells and enteroendocrine cells in the jejunum of d 0 and 7 piglets. Representative immunohistochemical images of piglet jejunum show goblet cells (A and B), enteroendocrine cells (E and F). Goblet cells are blue both in villus and crypt using AB-PAS staining and are marked by arrows. Enteroendocrine cells are brown in villus and crypt using the anti-CgA antibody and are marked by arrows. Quantitative analysis of goblet cells and enteroendocrine cells was displayed (C and D) and (G and H). The values in the figure are expressed as the mean and SEM ($n = 18$); differences were assessed by Student's t-test. Values at $P < 0.10$ show a tendency toward differing (100× magnification; scale bar, 200 μm). AB-PAS = Alcian blue-periodic acid-Schiff staining; CgA = Chromogranin A.

4. Discussion

The intestine develops rapidly in suckling pigs with dramatic changes in the length, width, density, shape of villi, and the depth of crypts (Skrzypek et al., 2018). Morphological measurements of the small intestine aged 0 and 7 d revealed dramatic changes in the jejunum CD and crypt fission index of piglets. Jejunal VH of 7-d-old piglets decreased significantly compared to that of 0-d-old piglets but small intestine CD increased significantly, resulting in a lower VH:CD. Reduced jejunal VH of 7-d-old piglets was validated by lower mRNA expression of *Villin* on d 7 jejunal tissue. Small intestine villus width increased significantly on d 7. Further, the number of crypts in the ileum increased significantly on d 7, but the crypt fission index in the duodenum and jejunum decreased dramatically. These morphologic distinctions have also been discovered in previous studies (Xu et al., 1992; Skrzypek et al., 2005, 2018). This experiment also found a greater crypt number in the ileum, indicating fast ileum growth and development of neonatal piglets, which is accompanied by crypt fission, namely, the increase of ISC for normal intestinal mucosa growth and/or regeneration (Dehmer et al., 2011; Langlands et al., 2016). Crypt fission is faster at an early developmental stage but slows down as the animal ages (Słupecka et al., 2010). It remains to be investigated whether the intestinal epithelium development in neonatal piglets is associated with the change in progenitors.

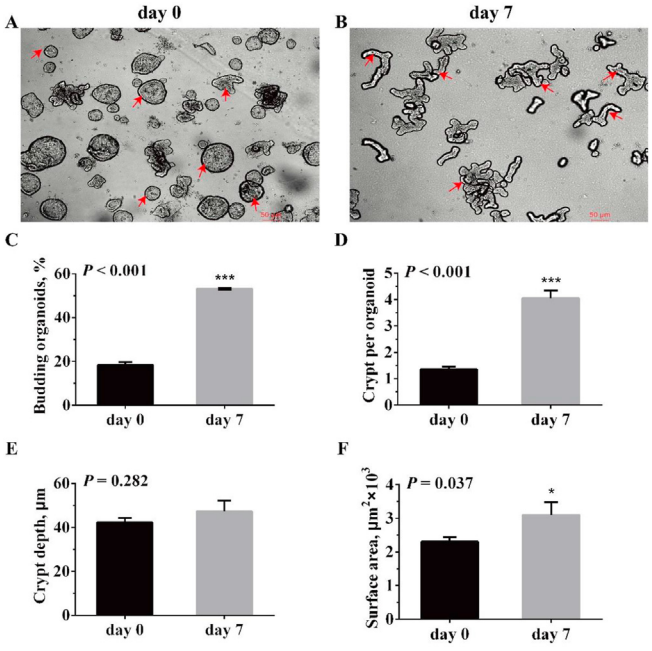

Fig. 4. The intestinal stem cell activity in d 0 and 7 piglets. Representative images of enteroids expanded from crypt stem cells of neonatal piglets on d 0 (A) and d 7 (B) of age after isolation for 5 d. The budding efficiency (C), crypts per enteroid (D), crypt depth (E), and surface area (F) at d 5 of culture were quantified. Results are expressed as the mean and SEM ($n = 4$). Differences were assessed by Student's t-test and denoted as follows: $^{*}P < 0.05$, $^{***}P < 0.001$. Representative images: d 5 primary crypt stem cells; arrows in A, B denote spheroids and organoids, respectively (50× magnification; scale bars, 50 μm). Statistics are based on 'n' biological replicates. All ex vivo experiments were performed at least twice with several wells under each condition, and sample material was chosen from at least 2 different piglets to take intra-individual and intra-experimental variation into account.

Piglet intestinal epithelium undergoes a complete renewal every 2 to 3 d driven by ISC located at the crypt base, which generates the precursors for the specialized differentiated cells (Verdile et al., 2019). Enteroids cultured from ISC partially recreate the villus-crypt anatomy of the native intestine and mimic hallmarks of in vivo epithelium (Yin et al., 2019a, 2019b). The activity of enteroids was determined by organoid budding efficiency, crypt depth, the number of crypts per organoid, and the surface area (Lindemans et al., 2015; Li et al., 2019c). Enteroids have been cultured to investigate the effects of diet and nutrients on intestinal epithelium development and the tissue-specific mechanisms by which Wnt-mediated signaling controls tissue renewal by regulating stem and progenitor cell activities as well as cell fate specification (Yin et al., 2019a; Merenda et al., 2020). To examine whether the intestinal epithelium development in neonatal piglets is associated with the change in progenitors, the primary ISC were cultured, and the ISC activity was measured. Cultivation of crypt ISC from 0-d-old piglets resulted in a mass of hollow spheroids without budding and branching structures primarily composed of stem cells. This finding is similar to those found in previous studies on fetal epithelium (Fordham et al., 2013; Mustata et al., 2013). In other studies, the crypts would be reprogrammed to a

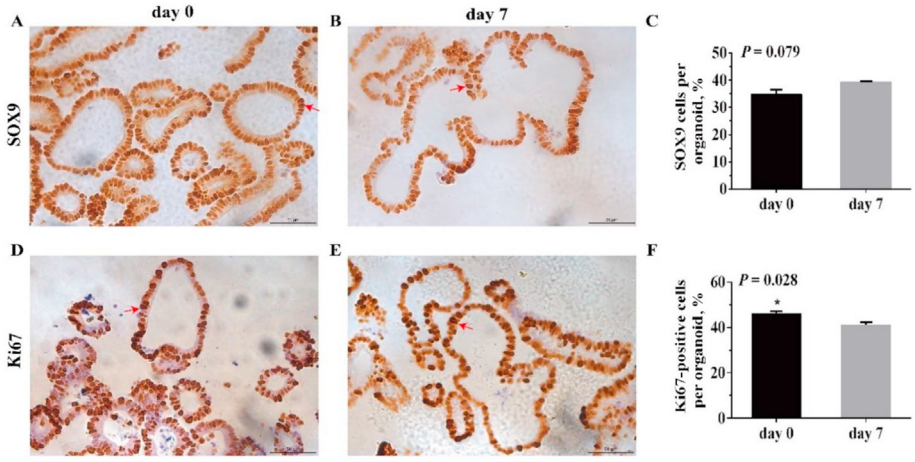

Fig. 5. Intestinal stem cell, and cell proliferation in jejunal enteroids on d 0 and 7. Representative immunohistochemical images of piglet jejunal enteroids show ISC (A and B), and proliferating cells (D and E) (400× magnification, scale bar, 50 μm). Intestinal stem cells and proliferating cells are dark brown in the crypt using the anti-SOX9, anti-Ki67 antibody respectively and are marked by red arrows. Quantitative analysis of the ratio of ISC, and proliferating cells was displayed (C and F). Cell nuclei were stained with hematoxylin. The ratio of the number of positive cells to total cell nuclei stained with hematoxylin is calculated. Values in the figure are expressed as means and SEM ($n = 4$); differences were assessed by Student's *t*-test and denoted as follows: $^*P < 0.05$. Values at $P < 0.10$ show a tendency toward differing. SOX9 = sex-determining region Y-box transcription factor 9.

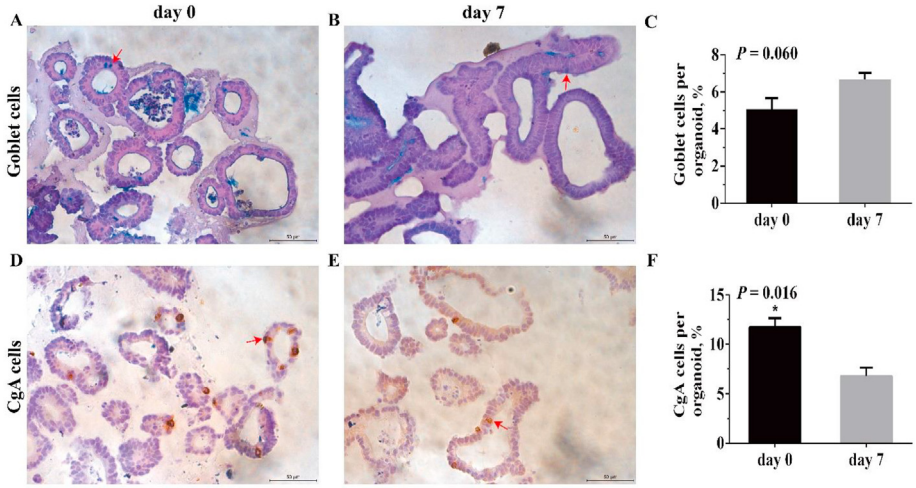

Fig. 6. Goblet cells and enteroendocrine cells in jejunal enteroids on d 0 and 7. Representative immunohistochemical images of piglet jejunal enteroids show goblet cells (A and B) and enteroendocrine cells (D and E) (400× magnification; scale bar, 50 μm). Goblet cells are blue using AB-PAS staining and are marked by arrows. Enteroendocrine cells are brown using the anti-CgA antibody and are marked by arrows. Quantitative analysis of the ratio of goblet cells, and enteroendocrine cells was displayed (C and F). Cell nuclei were stained with hematoxylin. The ratio of the number of positive cells to total cell nuclei stained with hematoxylin is calculated. Values in the figure are expressed as means and SEM ($n = 4$); differences were assessed by Student's *t*-test and denoted as follows: $^*P < 0.05$. Values at $P < 0.10$ show a tendency toward differing. CgA = chromogranin A; AB-PAS = Alcian blue-periodic acid-Schiff.

primitive state with fetal-like properties in response to tissue damage (Pont and Yan, 2018; Yui et al., 2018), suggesting that fetal progenitors may be linked with the rapid proliferation and division of crypts. Cultivation of crypt ISC from 7-d-old piglets led to a substantial number of organoids with budding and branching structures. The adult small intestinal epithelium is composed of differentiated villi and proliferating crypts. Adult ISC divide to generate more stem cells that give rise to rapidly proliferating TA cells that differentiate into four major mature cell types, namely, the absorptive enterocytes, the goblet cells, the enteroendocrine cells, and Paneth cells (Clevers et al., 2014), which may be responsible for the greater total crypts number on d 7. The difference was reflected in the organoid budding efficiency, crypt domains per organoid, and surface area. Moreover, cellular migration and regeneration are slower in the intestine of suckling animals than in adult animals (Koldovsky et al., 1966).

ISC can spontaneously generate all differentiated cell types, contributing to maintaining intestinal epithelium homeostasis (Gehart and Clevers, 2019). We first distinguished stem/progenitor cells from d 0 and 7 both in tissues and organoids. Unfortunately, Lgr5, the commercially available antibody used to detect the ISC population, did not demonstrate cross-reactivity with ISC in porcine jejunal tissue (data not shown), as demonstrated in the previous study (Gonzalez et al., 2013), only SOX9 displayed positive staining. SOX9, located at the bottom of the crypt and expressed in ISC and TA cells (Verdile et al., 2019), was also considered as the ISC marker. The number of $SOX9^+$ cells increased in jejunal tissue on d 7 in the current study, which was consistent with the jejunum of suckling piglets on d 6 after birth in Verdile et al. (2019). Furthermore, $SOX9^+$ cells were higher on d 7 organoids, which confirmed the reduction of the CBC signature in spheroids (Mustata et al., 2013). These data were validated by the expression of adult stem

Table 3
The mRNA expression of related marker genes in jejunal tissues of neonatal piglets in vivo.[1]

Item[2]	Day after birth		*P*-value
	0 d	7 d	
Epithelial-specific markers			
Villin	1.01 ± 0.07	0.82 ± 0.06	0.089
E-cadherin	1.02 ± 0.12	0.88 ± 0.04	0.304
TJP1	1.01 ± 0.09	0.90 ± 0.08	0.379
Differentiation markers			
Alpi	1.04 ± 0.15	0.86 ± 0.05	0.311
Muc2	1.01 ± 0.10	0.94 ± 0.05	0.548
Lyz	1.73 ± 0.78	26.51 ± 11.96	0.130
ChgA	1.00 ± 0.03	0.83 ± 0.03	0.014
Fetal ISC markers			
Tacstd2	1.12 ± 0.32	1.16 ± 0.15	0.903
Gja1	1.02 ± 0.11	0.83 ± 0.13	0.313
Adult ISC markers			
Lgr5	1.04 ± 0.18	0.99 ± 0.13	0.830
Smoc2	1.07 ± 0.22	2.65 ± 0.47	0.022
Cdx1	1.03 ± 0.14	0.99 ± 0.11	0.858

[1] The values are expressed as mean ± SEM ($n = 18$). Differences were assessed by the Student's *t*-test. Values of $P < 0.05$ are referred to as statistically significant.
[2] *TJP1* = tight junction protein 1; *Alpi* = alkaline phosphatase; *Muc2* = mucin 2; *Lyz* = lysozyme; *ChgA* = chromogranin A; ISC = intestinal stem cells; *Tacstd2* = tumor associated calcium signal transducer 2; *Gja1* = gap junction protein, alpha 1; *Smoc2* = SPARC related modular calcium binding 2; *Cdx1* = caudal type homeobox 1; *Lgr5* = leucine-rich repeat-containing G protein-coupled receptor 5.

Table 4
The mRNA expression of related marker genes in enteroids expanded from crypt stem cells of neonatal piglets in vitro.[1]

Item[2]	Day after birth		*P*-value
	0 d	7 d	
Epithelial-specific markers			
Villin	1.01 ± 0.08	1.53 ± 0.14	0.029
E-cadherin	1.16 ± 0.38	2.70 ± 0.18	0.022
TJP1	2.09 ± 1.30	2.90 ± 0.10	0.564
Differentiation markers			
Alpi	1.02 ± 0.15	1.19 ± 0.13	0.433
Muc2	1.05 ± 0.24	2.25 ± 0.39	0.059
Lyz	1.28 ± 0.33	85.38 ± 24.75	0.019
ChgA	1.01 ± 0.06	0.51 ± 0.11	0.002
Fetal ISC markers			
Tacstd2	1.06 ± 0.23	0.65 ± 0.27	0.312
Gja1	1.19 ± 0.27	0.43 ± 0.28	0.021
Spp1	1.41 ± 0.84	0.87 ± 0.27	0.571
Adult ISC markers			
Lgr5	1.12 ± 0.27	10.59 ± 2.18	<0.001
Smoc2	1.00 ± 0.04	4.09 ± 0.42	<0.001
Cdx1	1.01 ± 0.09	1.13 ± 0.26	0.680

[1] The values are expressed as mean ± SEM ($n = 4$). Differences were assessed by the Student's *t*-test. Values of $P < 0.05$ are referred to as statistically significant.
[2] *TJP1* = tight junction protein 1; *Alpi* = alkaline phosphatase; *Muc2* = mucin 2; *Lyz* = lysozyme; *ChgA* = chromogranin A; ISC = intestinal stem cells; *Tacstd2* = tumor associated calcium signal transducer 2; *Gja1* = gap junction protein, alpha 1; *Spp1* = secreted phosphoprotein 1; *Smoc2* = SPARC related modular calcium binding 2; *Cdx1* = caudal type homeobox 1; *Lgr5* = leucine-rich repeat-containing G protein-coupled receptor 5.

cell markers using RT-qPCR: *Smoc2* were down-regulated on d 0 jejunal tissue, *Lgr5* and *Smoc2* were also down-regulated in spheroids. Ki67, a marker for cell proliferation, labeled the undifferentiated proliferating TA cells (progenitors) at the crypt (Beyaz et al., 2016; Ito et al., 2020). The present study indicated that spheroids displayed proliferating cells all over their surface and represented a high proliferation phenotype. However, proliferating cells in organoids were restricted to crypt-like protrusions, which coincided with the finding of Mustata et al. (2013). To further investigate the expression of major secretory cells in jejunal tissues

Table 5
The mRNA expression of genes involved in related signaling pathways in jejunal tissues of neonatal piglets in vivo.[1]

Item[2]	Day after birth		*P*-value
	0 d	7 d	
Wnt/β-catenin signaling			
Jag-1	1.09 ± 0.24	0.42 ± 0.01	0.069
Jag-2	1.04 ± 0.16	0.76 ± 0.08	0.177
Sgk1	1.17 ± 0.34	0.40 ± 0.07	0.109
Bmp4	1.01 ± 0.08	0.72 ± 0.05	0.020
Nedd8	1.01 ± 0.06	0.56 ± 0.01	0.004
Ephb4	1.02 ± 0.11	1.00 ± 0.10	0.907
C-Myc	1.04 ± 0.15	1.17 ± 0.20	0.598
Ccnd1	1.02 ± 0.12	0.92 ± 0.08	0.486
Axin2	1.01 ± 0.07	0.71 ± 0.07	0.026
EGF signaling			
EGFR	1.04 ± 0.17	1.07 ± 0.11	0.885
Notch signaling			
Notch1	1.04 ± 0.18	0.94 ± 0.13	0.683
Notch2	1.07 ± 0.21	1.07 ± 0.42	0.990
Atoch1	1.02 ± 0.12	1.22 ± 0.14	0.326
Hes1	1.03 ± 0.15	0.91 ± 0.09	0.503
Dll1	1.04 ± 0.16	0.73 ± 0.06	0.117
Dll4	1.02 ± 0.10	1.19 ± 0.11	0.279
BMP signaling			
Id1	1.06 ± 0.21	1.09 ± 0.08	0.901
Id2	1.03 ± 0.14	1.01 ± 0.08	0.894
Bmpr1a	1.04 ± 0.17	1.37 ± 0.07	0.119
Bmp2	1.07 ± 0.22	1.34 ± 0.11	0.332
Smad4	1.03 ± 0.15	0.98 ± 0.09	0.804

[1] The values are expressed as mean ± SEM ($n = 18$). Differences were assessed by the Student's *t*-test. Values of $P < 0.05$ are referred to as statistically significant.
[2] *Notch1* = Notch receptor 1; *Notch2* = Notch receptor 2; *Atoh1* = atonal bHLH transcription factor 1; *Hes1* = hes family bHLH transcription factor 1; *Dll1* = delta like canonical Notch ligand 1; *Dll4* = delta like canonical Notch ligand 4; *Jag1* = jagged canonical Notch ligand 1; *Jag2* = jagged canonical Notch ligand 2; *Sgk1* = serum/glucocorticoid regulated kinase 1; *Bmp4* = bone morphogenetic protein 4; *Nedd8* = neural precursor cell expressed developmentally down-regulated 8; *Ephb4* = EPH receptor B4; *Axin2* = axis inhibition protein 2; *EGFR* = epidermal growth factor receptor; *Ccnd1* = cyclin D1; *Id1* = inhibitor of DNA binding 1; *Id2* = inhibitor of DNA binding 2; *Smad4* = SMAD family member 4; Bmp2 = bone morphogenetic protein 2; *Bmpr1a* = bone morphogenetic protein receptor type 1a.

and organoids, we used AB-PAS staining, anti-lysozyme, and anti-CgA antibody to measure the number of goblet cells, Paneth cells, and enteroendocrine cells. Previous studies have shown that spheroids exhibited low expression of differentiation markers (Mustata et al., 2013). Similarly, in our study, goblet cells in spheroids tended to decrease, but enteroendocrine cells in spheroids and jejunal tissues tended to increase on d 0, and this result was interesting and confirmed by RT-qPCR. *ChgA*, the enteroendocrine cells marker, was down-regulated in spheroids and jejunal tissue on d 0. Paneth cells, located between CBC cells, secreted lysozyme and, in mice, can be identified by anti-lysozyme antibodies in the small intestine (Hageman et al., 2020; Sato et al., 2011). The presence of Paneth cells remains controversial in the intestine of piglets (Gonzalez et al., 2013). However, in our present study, lysozyme-positive cells were detected between the very bottom of the crypt and the muscular mucosa but were not detected in the crypt (data not shown).

To better understand the differences between spheroids and organoids, the mRNA expression of epithelial-specific markers such as *Villin* and *E-cadherin*, tight junction protein 1 (*TJP1*) in jejunal organoids was measured to demonstrate that the cells isolated were of epithelial origin (Mustata et al., 2013). The mRNA expression of *Villin* and *E-cadherin* in the jejunal organoid cultured from 7-d-old piglets was up-regulated compared to that of 0-d-old piglets. To characterize the different ISC phenotypes, the fetal ISC markers such as secreted phosphoprotein 1 (*Spp1*), the cell surface molecule

Table 6
The mRNA expression of genes involved in related signaling pathways in enteroids expanded from crypt stem cells of neonatal piglets in vitro.[1]

Item[2]	Day after birth		*P*-value
	0 d	7 d	
Wnt/β-catenin signaling			
Jag-1	1.05 ± 0.22	3.65 ± 0.07	<0.001
Jag-2	1.01 ± 0.09	2.70 ± 0.48	0.025
Sgk1	1.07 ± 0.24	1.05 ± 0.07	0.966
Bmp4	1.15 ± 0.40	2.17 ± 0.20	0.085
Nedd8	1.03 ± 0.18	1.80 ± 0.21	0.047
Ephb4	1.01 ± 0.10	1.96 ± 0.08	0.002
C-Myc	1.00 ± 0.03	2.91 ± 0.10	<0.001
Ccnd1	1.03 ± 0.17	2.21 ± 0.03	0.002
Axin2	1.02 ± 0.14	2.69 ± 0.21	0.003
EGF signaling			
EGFR	1.03 ± 0.18	2.75 ± 0.14	0.002
Notch signaling			
Notch1	1.04 ± 0.14	3.00 ± 0.62	0.001
Notch2	1.07 ± 0.25	0.46 ± 0.17	0.116
Atoch1	1.04 ± 0.22	0.85 ± 0.12	0.493
Hes1	1.04 ± 0.19	2.55 ± 0.17	0.004
Dll1	1.00 ± 0.08	4.46 ± 0.88	0.056
Dll4	1.00 ± 0.05	1.15 ± 0.13	0.367
BMP signaling			
Id1	1.07 ± 0.17	1.28 ± 0.12	0.326
Id2	1.01 ± 0.07	1.12 ± 0.06	0.274
Bmpr1a	1.10 ± 0.30	3.55 ± 0.27	0.004
Bmp2	1.02 ± 0.14	1.46 ± 0.15	0.098
Smad4	1.04 ± 0.20	3.17 ± 0.22	0.002

[1] The values are expressed as mean ± SEM ($n = 4$). Differences were assessed by the Student's *t*-test. Values of $P < 0.05$ are referred to as statistically significant.

[2] *Notch1* = Notch receptor 1; *Notch2* = Notch receptor 2; *Atoh1* = atonal bHLH transcription factor 1; *Hes1* = hes family bHLH transcription factor 1; *Dll1* = delta like canonical Notch ligand 1; *Dll4* = delta like canonical Notch ligand 4; *Jag1* = jagged canonical Notch ligand 1; *Jag2* = jagged canonical Notch ligand 2; *Sgk1* = serum/glucocorticoid regulated kinase 1; *Bmp4* = bone morphogenetic protein 4; *Nedd8* = neural precursor cell expressed developmentally down-regulated 8; *Ephb4* = EPH receptor B4; *Axin2* = axis inhibition protein 2; *EGFR* = epidermal growth factor receptor; *Ccnd1* = cyclin D1; *Id1* = inhibitor of DNA binding 1; *Id2* = inhibitor of DNA binding 2; *Smad4* = SMAD family member 4; Bmp2 = bone morphogenetic protein 2; *Bmpr1a* = bone morphogenetic protein receptor type 1a.

Trop2, also known as Tumour-associated calcium signal transducer 2 (*Tacstd2*) (Fernandez Vallone et al., 2016), *Gja1*/*Cx43*/*Cnx43* genes (referred to as *Cnx43*) (Pont and Yan, 2018) and additional adult ISC markers such as *Lgr5*/*Gpr49*, *Smoc2*, *Axin2*, caudal type homeobox 1 (*Cdx1*) were examined to determine that the cells isolated were of different stem cell types (Mustata et al., 2013). There was an up-regulation of adult ISC markers genes, but a down-regulation of fetal ISC markers genes on d 7. Spheroids indicate poorly differentiated phenotypes (Mustata et al., 2013). Differentiation markers for corresponding genes were detected, namely, alkaline phosphatase (*Alpi*) for absorptive enterocytes, *Muc2* for goblet cell, *Lyz* for Paneth cell, and *ChgA* for enteroendocrine cell (van der Flier and Clevers, 2009; Yui et al., 2018; Hageman et al., 2020). Our study demonstrated that spheroids showed lower mRNA expression of *Lyz* and *Muc2*, which is consistent with the findings in the previous study. The mRNA expression of *ChgA* was significantly up-regulated on d 0, and the underlying mechanism needs to be explored. It has been proved that the epithelium was transiently reprogrammed to a primitive state with higher expression of fetal markers and suppression of adult stem cells and differentiated cells markers (Yui et al., 2018). The 2 temporally distinct types of stem/progenitor cells were distinguished by gene expression and differential mechanisms of regulation.

Several pathways are crucial to maintain and regulate ISC, including Wnt, Notch, BMP, and EGF (Yeung et al., 2011; Beumer and Clevers, 2021). To explore the potential mechanism of ISC differentiation and self-renewal, related genes in these signaling pathways were detected in vivo and in vitro. The Wnt/β-catenin pathway is required for regulating cell fate along the crypt-villus axis in the normal intestinal epithelium and ISC self-renewal, in which β-catenin target genes such as *Bmp4*, *Jag1*, *Jag2*, endothelin 3 (*Edn3*), *Ephb4*, *Nedd8*, serum/glucocorticoid regulated kinase 1 (*Sgk1*), *c-Myc*, *Ccnd1*, and *Axin2* evoked expression to maintain the proliferation of ISC and progenitors (Yeung et al., 2011; Beyaz et al., 2016; Tian et al., 2017). EGF signaling is pivotal for ISC proliferation and acts through the EGF receptor (Beumer and Clevers, 2021). Furthermore, the Notch pathway is vital to induce the progenitor cell differentiation into secretory lineage cells, in which *Hes1* and *Atoh1* are the main transcription targets, and the fate of ISC was determined by up-regulating the expression of *Hes1* and inhibiting atonal bHLH transcription factor 1 (*Atoh1*) (Zhou et al., 2021). BMP belongs to the transforming growth factor-β family, and this pathway is known to inhibit the canonical Wnt pathway, proliferation, and promote progenitor cells differentiation (Tian et al., 2017). Bmp2 and Bmp4 are the main BMPs and its receptor Bmpr1a and SMADs are expressed along the villus (Yeung et al., 2011; Beumer and Clevers, 2021). The present study indicated that target genes of β-catenin were up-regulated on d 0 jejunal tissue, but down-regulated on d 0 spheroids. Porcine mini-guts were embedded in Matrigel supplemented with growth factors, such as Wnt3a, the Wnt signal enhancer R-spondin, BMP inhibitor Noggin, GSK3i (CHIR99021, Wnt agonist), and EGF, which provided enough Wnt ligands for organoids growth (Khalil et al., 2016). However, spheroids respond complicatedly to Wnt stimulation, and fetal spheroid cells possibly because of their different epigenetic status, or crosstalk with different concurrent regulatory cascades (Mustata et al., 2013). Accordingly, inhibition of the Wnt/β-catenin pathway on d 0 spheroids was shown possibly as a result of the niche that was supplemented with the Wnt ligands, and spheroids and organoids respond differently to this. What's more, Notch ligands are presented mainly by neighboring Paneth cells, and its marker gene, *Lyz*, was up-regulated on d 7 organoids, which resulted in activation of Notch signaling. The Notch pathway was beneficial to the proliferation of adult ISC and contributed to the maintenance of spheroid progenitor cells in an undifferentiated state (Noah and Shroyer, 2013). Fre et al. (2005) noted that Notch activation inhibited the differentiation of enteroendocrine cells in the intestine of mice, which might have been responsible for the marked reduction of the number of CgA cells on d 7 organoids. More importantly, inhibition of BMP signaling impairs the secretory lineage differentiation, and loss of Bmpr1a also leads to reduction in terminal differentiation of Paneth cells with down-regulated expression of lysozyme markers (Auclair et al., 2007). Genes involved in the BMP signaling pathway were down-regulated on spheroids, which suggested the inhibition of BMP signaling, and which might have down-regulated the mRNA expression of *Lyz* in the current study.

The different nutritional and metabolic characteristics between fetal progenitors and $Lgr5^{+}$ ISC indicated the potential of nutrients to regulate the conversion of ISC. Accordingly, our results may provide a vital theoretical basis for nutritional regulation of intestinal development in neonatal piglets. Moreover, spheroids can be converted into organoids with budding and branching structures under long-term and stable culture medium in mice (Navis et al., 2019; Garcia et al., 2019), which indicated that the piglet's spheroids provide a model for the investigation of the process of gut maturation and developing different kind of modulators, such as nutrients, to promote the intestinal development and fast growth.

Significant advances have been made in murine ISC biology. However, differences between mice and humans in anatomy and

physiology have limited mice used as a proper model for stem cell study. Since pig and human intestines share many similarities in the genetic, anatomical, and physiological properties (Yin et al., 2019b), the porcine enteroid model is considered an appropriate platform for developing medicines treating human gastrointestinal diseases. Moreover, Li et al. (2019b) have reported that porcine enteroids provide a novel in vitro model for exploring the pathogenesis of porcine epidemic diarrhea virus (PEDV) and the interactions between a host and various porcine enteric viruses. Notably, porcine has been an effective translational model and a candidate species to study the regeneration driven by intestinal epithelial stem cells (Gonzalez et al., 2013). Additionally, a method for the long-term culture of porcine crypts was developed. The porcine intestinal organoid is a promising model to study stem cell-driven regeneration of the intestinal epithelium in vitro.

5. Conclusion

This study found that crypt fission decreases with the increase of animal age because of the conversion from fetal ISC (spheroids) to adult ISC (normal organoids). Notably, fetal progenitors are associated with the fast proliferation of crypts, suggesting that fetal stem cells better enhance regeneration. It also found that the conversion from the fetal progenitors to adult ISC might largely be responsible for the fast intestine development in neonatal piglets. These findings carry significant implications for analyzing the intestinal development mechanism of newborn piglets and developing new nutritional intervention strategies.

Author contributions

Lanmei Yin: Investigation, Data curation, Writing – original draft preparation. **Jun Li**: Visualization, Investigation, Formal analysis. **Yitong Zhang**: Data curation, Supplement experiment. **Qing Yang**: Investigation, Validation, **Cuiyan Yang**: Investigation, Validation. **Zhenfeng Yi**: Investigation, Validation. **Yuebang Yin**: Resources. **Qiye Wang**: Visualization. **Jianzhong Li:** Project administration. **Huansheng Yang**: Conceptualization, Methodology, Software, Writing – review & editing. **Yulong Yin**: Supervision, Funding acquisition, Writing – review & editing.

Declaration of competing interest

We declare that we have no financial and personal relationships with other people or organizations that can inappropriately influence our work, and there is no professional or other personal interest of any nature or kind in any product, service and/or company that could be construed as influencing the content of this paper.

Acknowledgements

This study was supported by National Key R & D Program (2016YFD0501201), Key Programs of frontier scientific research of the Chinese Academy of Sciences (QYZDY-SSWSMC008), Changsha Zhuzhou Xiangtan High-level Talent Concentration Project (2017XK2022), Tianjin Synthetic Biotechnology Innovation Capacity Improvement Project (TSBICIP-CXRC-038).

References

Auclair BA, Benoit YD, Rivard N, Mishina Y, Perreault N. Bone morphogenetic protein signaling is essential for terminal differentiation of the intestinal secretory cell lineage. Gastroenterology 2007;133(3):887–96.

Beumer J, Clevers H. Cell fate specification and differentiation in the adult mammalian intestine. Nat Rev Mol Cell Biol 2021;22(1):39–53.

Beyaz S, Mana MD, Roper J, Kedrin D, Saadatpour A, Hong SJ, et al. High-fat diet enhances stemness and tumorigenicity of intestinal progenitors. Nature 2016;531(7592):53–8.

Buczacki SJ, Zecchini HI, Nicholson AM, Russell R, Vermeulen L, Kemp R, et al. Intestinal label-retaining cells are secretory precursors expressing Lgr5. Nature 2013;495(7439):65–9.

Clevers H, Loh LM, Nusse R. An integral program for tissue renewal and regeneration: Wnt signaling and stem cell control. Science 2014;346(6205):1248012.

Dehmer JJ, Garrison AP, Speck KE, Dekaney CM, Van Landeghem L, Sun X, et al. Expansion of intestinal epithelial stem cells during murine development. PLoS One 2011;6(11):e27070.

Dehmer JJ, Garrison AP, Speck KE, Dekaney CM, Van Landeghem L, Sun X, et al. Expansion of intestinal epithelial stem cells during murine development. PLoS One 2011;6(11):e27070.

Deng Q, Shao Y, Wang Q, Li J, Li Y, Ding X, et al. Effects and interaction of dietary electrolyte balance and citric acid on the intestinal function of weaned piglets. J Anim Sci 2020;98(5). skaa106.

Fernandez Vallone V, Leprovots M, Strollo S, Vasile G, Lefort A, Libert F, et al. Trop2 marks transient gastric fetal epithelium and adult regenerating cells after epithelial damage. Development 2016;143(9):1452–63.

Fordham RP, Yui S, Hannan NR, Soendergaard C, Madgwick A, Schweiger PJ, et al. Transplantation of expanded fetal intestinal progenitors contributes to colon regeneration after injury. Cell Stem Cell 2013;13(6):734–44.

Fre S, Huyghe M, Mourikis P, Robine S, Louvard D, Artavanis-Tsakonas S. Notch signals control the fate of immature progenitor cells in the intestine. Nature 2005;435(7044):964–8.

Garcia TM, Navis M, Wildenberg ME, van Elburg RM, andMuncan V. Recapitulating suckling-to-weaning transition in vitro using fetal intestinal organoids. JoVE 2019;153:e60470.

Gehart H, Clevers H. Tales from the crypt: new insights into intestinal stem cells. Nat Rev Gastroenterol Hepatol 2019;16(1):19–34.

Gonzalez LM, Williamson I, Piedrahita JA, Blikslager AT, Magness ST. Cell lineage identification and stem cell culture in a porcine model for the study of intestinal epithelial regeneration. PLoS One 2013;8(6):e66465.

Hageman JH, Heinz MC, Kretzschmar K, van der Vaart J, Clevers H, Snippert HJG. Intestinal regeneration: regulation by the microenvironment. Dev Cell 2020;54(4):435–46.

Ito S, Nada S, Yamazaki D, Kimura T, Kajiwara K, Miki H, et al. p18/Lamtor1-mTORC1 signaling controls development of mucin-producing goblet cells in the intestine. Cell Struct Funct 2020;45(2):93–105.

Jones JC, Dempsey PJ. Enterocyte progenitors can dedifferentiate to replace lost Lgr5^{+} intestinal stem cells revealing that many different progenitor populations can regain stemness. Stem Cell Invest 2016;3:61.

Khalil HA, Lei NY, Brinkley G, Scott A, Wang J, Kar UK, et al. A novel culture system for adult porcine intestinal crypts. Cell Tissue Res 2016;365(1):123–34.

Koldovsky O, Sunshine P, Kretchmer N. Cellular migration of intestinal epithelia in suckling and weaned rats. Nature 1966;212(5068):1389–90.

Langlands AJ, Almet AA, Appleton PL, Newton IP, Osborne JM, Näthke IS. Paneth cell-rich regions separated by a cluster of Lgr5+ cells initiate crypt fission in the intestinal stem cell niche. PLoS Biol 2016;14(6):e1002491.

Li J, Yin L, Wang L, Li J, Huang P, Yang H, et al. Effects of vitamin B6 on growth, diarrhea rate, intestinal morphology, function, and inflammatory factors expression in a high-protein diet fed to weaned piglets. J Anim Sci 2019a;97(12):4865–74.

Li L, Fu F, Guo S, Wang H, He X, Xue M, et al. Porcine intestinal enteroids: a new model for studying enteric coronavirus porcine epidemic diarrhea virus infection and the host innate response. J Virol 2019b;93(5). 01682-01618.

Li XG, Zhu M, Chen MX, Fan HB, Fu HL, Zhou JY, et al. Acute exposure to deoxynivalenol inhibits porcine enteroid activity via suppression of the Wnt/β-catenin pathway. Toxicol Lett 2019c;305:19–31.

Lindemans CA, Calafiore M, Mertelsmann AM, O'Connor MH, Dudakov JA, Jenq RR, et al. Interleukin-22 promotes intestinal-stem-cell-mediated epithelial regeneration. Nature 2015;528(7583):560–4.

Merenda A, Fenderico N, Maurice MM. Wnt signaling in 3D: recent advances in the applications of intestinal organoids. Trends Cell Biol 2020;30(1):60–73.

Mustata RC, Vasile G, Fernandez-Vallone V, Strollo S, Lefort A, Libert F, et al. Identification of Lgr5-independent spheroid-generating progenitors of the mouse fetal intestinal epithelium. Cell Rep 2013;5(2):421–32.

Navis M, Martins Garcia T, Renes IB, Vermeulen JL, Meisner S, Wildenberg ME, et al. Mouse fetal intestinal organoids: new model to study epithelial maturation from suckling to weaning. EMBO Rep 2019;20(2):e46221.

Noah TK, Shroyer NF. Notch in the intestine: regulation of homeostasis and pathogenesis. Annu Rev Physiol 2013;75:263–88.

Park HS, Goodlad RA, Ahnen DJ, Winnett A, Sasieni P, Lee CY, et al. Effects of epidermal growth factor and dimethylhydrazine on crypt size, cell proliferation, and crypt fission in the rat colon: cell proliferation and crypt fission are controlled independently. Am J Pathol 1997;151(3):843–52.

Pierson H, Yang H, Lutsenko S. Copper transport and disease: what can we learn from organoids? Annu Rev Nutr 2019;39:75–94.

Pont AR, Yan KS. Intestinal crypts assume the fetal position in response to injury. Cell Stem Cell 2018;23(2):158–9.

Powell RH, Behnke MS. WRN conditioned media is sufficient for in vitro propagation of intestinal organoids from large farm and small companion animals. Biol Open 2017;6(5):698–705.
Pu Y, Li S, Xiong H, Zhang X, Wang Y, Du H. Iron promotes intestinal development in neonatal piglets. Nutrients 2018;10(6):726.
Ren W, Yin J, Wu M, Liu G, Yang G, Xion Y, et al. Serum amino acids profile and the beneficial effects of L-arginine or L-glutamine supplementation in dextran sulfate sodium colitis. PLoS One 2014;9(2):e88335.
Sato T, van Es JH, Snippert HJ, Stange DE, Vries RG, van den Born M, et al. Paneth cells constitute the niche for Lgr5 stem cells in intestinal crypts. Nature 2011;469(7330):415–8.
Skrzypek T, Valverde Piedra JL, Skrzypek H, Woliński J, Kazimierczak W, Szymańczyk S, et al. Light and scanning electron microscopy evaluation of the postnatal small intestinal mucosa development in pigs. J Physiol Pharmacol 2005;56(Suppl 3):71–87.
Skrzypek TH, Kazimierczak W, Skrzypek H, Valverde Piedra JL, Godlewski MM, Zabielski R. Mechanisms involved in the development of the small intestine mucosal layer in postnatal piglets. J Physiol Pharmacol 2018;69(1):127–38.
Słupecka M, Woliński J, Pierzynowski SG. Crypt fission contributes to postnatal epithelial growth of the small intestine in pigs. Livest Sci 2010;133:34–7.
Tian Y, Ma X, Lv C, Sheng X, Li X, Zhao R, et al. Stress responsive miR-31 is a major modulator of mouse intestinal stem cells during regeneration and tumorigenesis. eLife 2017;6:e29538.
van der Flier LG, Clevers H. Stem cells, self-renewal, and differentiation in the intestinal epithelium. Annu Rev Physiol 2009;71:241–60.
Van Lidth de Jeude JF, Vermeulen JL, Montenegro-Miranda PS, Van den Brink GR, Heijmans J. A protocol for lentiviral transduction and downstream analysis of intestinal organoids. JoVE 2015;(98):e52531. JoVE.
Verdile N, Mirmahmoudi R, Brevini TAL, Gandolfi F. Evolution of pig intestinal stem cells from birth to weaning. Animal 2019;13(12):2830–9.
Wang LX, Zhu F, Li JZ, Li YL, Ding XQ, Yin J, et al. Epidermal growth factor promotes intestinal secretory cell differentiation in weaning piglets via Wnt/β-catenin signaling. Animal 2020a;14(4):790–8.
Wang Z, Li J, Wang Y, Wang L, Yin Y, Yin L, et al. Dietary vitamin A affects growth performance, intestinal development, and functions in weaned piglets by affecting intestinal stem cells. J Anim Sci 2020b;98(2):skaa020.
Xiong X, Yang HS, Wang XC, Hu Q, Liu CX, Wu X, et al. Effect of low dosage of chitooligosaccharide supplementation on intestinal morphology, immune response, antioxidant capacity, and barrier function in weaned piglets. J Anim Sci 2015;93(3):1089–97.
Xu RJ, Mellor DJ, Tungthanathanich P, Birtles MJ, Reynolds GW, Simpson HV. Growth and morphological changes in the small and the large intestine in piglets during the first three days after birth. J Dev Physiol 1992;18(4):161–72.
Yan S, Long L, Zong E, Huang P, Li J, Li Y, et al. Dietary sulfur amino acids affect jejunal cell proliferation and functions by affecting antioxidant capacity, Wnt/β-catenin, and the mechanistic target of rapamycin signaling pathways in weaning piglets. J Anim Sci 2018;96(12):5124–33.
Yang HS, Xiong X, Yin YL. Development and renewal of intestinal villi in pigs. In: Nutritional and physiological functions of amino acids in pigs. Springer Vienna; 2013. p. 29–47.
Yeung TM, Chia LA, Kosinski CM, Kuo CJ. Regulation of self-renewal and differentiation by the intestinal stem cell niche. Cell Mol Life Sci 2011;68(15):2513–23.
Yin Y, Bijvelds M, Dang W, Xu L, van der Eijk AA, Knipping K, et al. Modeling rotavirus infection and antiviral therapy using primary intestinal organoids. Antivir Res 2015;123:120–31.
Yin YB, de Jonge HR, Wu X, Yin YL. Enteroids for nutritional studies. Mol Nutr Food Res 2019a;63(16):e1801143.
Yin YB, Guo SG, Wan D, Wu X, Yin YL. Enteroids: promising in vitro models for studies of intestinal physiology and nutrition in farm animals. J Agric Food Chem 2019b;67(9):2421–8.
Yin L, Li L, Wang H, Yi Z, Wang L, Zhang S, Li X, et al. Effects of vitamin B6 on the growth performance, intestinal morphology, and gene expression in weaned piglets that are fed a low-protein diet1. J Anim Sci 2020;98(2). skaa022.
Yui S, Azzolin L, Maimets M, Pedersen MT, Fordham RP, Hansen SL, et al. YAP/TAZ-dependent reprogramming of colonic epithelium links ECM remodeling to tissue regeneration. Cell Stem Cell 2018;22(1):35–49. e7.
Zhou J, Qin Y, Xiong X, Wang Z, Wang M, Wang Y, et al. 2021. Effects of iron, Vitamin A and the interaction between the two nutrients on intestinal development and cell differentiation in piglets. J Anim Sci 2021;99(10). skab258.
Zhou JY, Wang Z, Zhang SW, Lin HL, Gao CQ, Zhao JC, et al. Methionine and its hydroxyl analogues improve stem cell activity to eliminate deoxynivalenol-induced intestinal injury by reactivating wnt/β-catenin signaling. J Agric Food Chem 2019;67(41):11464–73.